CHEMISTRY & SUSTAINABILITY

CHEMSUSCHEM

ENERGY & MATERIALS

# Accepted Article

**Title:** Microwave-assisted decarbonylation of biomass-derived aldehydes using Pd-doped hydrotalcites

**Authors:** Nan An, Diana Ainembabazi, Christopher Reid, Kavya Samudrala, Karen Wilson, Adam F Lee, and Adelina Voutchkova-Kostal



**To be cited as:** *ChemSusChem* 10.1002/cssc.201901934

**Link to VoR:** http://dx.doi.org/10.1002/cssc.201901934

A Journal of

ChemPubSoc Europe

WILEY-VCH

www.chemsuschem.org

WILEY-VCH

FULL PAPER

# Microwave-assisted Decarbonylation of Biomass-derived Aldehydes using Pd-doped Hydrotalcites

Nan An[a], Diana Ainembabazi[a], Christopher Reid[a], Kavya Samudrala[a], Karen Wilson[b]

Adam F. Lee[b], Adelina Voutchkova-Kostal[a]

**Abstract:** Catalytic decarbonylation is an underexplored strategy for deoxygenation of biomass-derived aldehydes due to a lack of lowcost and robust heterogeneous catalysts able to operate in benign solvents. A family of Pd functionalized hydrotalcites (Pd-HTs) were synthesized, characterized, and applied to the decarbonylation of furfural, HMF, and aromatic and aliphatic aldehydes under microwave conditions. This catalytic system delivered enhanced decarbonylation yields and turnover frequencies, even at a low Pd loading (0.5 mol%). Furfural decarbonylation was optimized in a benign solvent (ethanol) compatible with biomass processing; HMF selectively affords excellent yields (93 %) of furfuryl alcohol without humin formation, however longer reaction favors furan via tandem alcohol dehydrogenation and decarbonylation. Yields of substituted benzaldehydes (37 - 99 %) were proportional to the calculated Mulliken charge of the carbonyl carbon. Activity and selectivity reflect loading-dependent Pd speciation. Continuous flow testing of the best Pd-HT catalyst delivered good stability over 16h on stream, with near-quantitative conversion of HMF.

## Introduction

Replacement of fossil fuel feedstocks for chemical and fuel production with alternative oxygenated biomass-derived sources requires the development of efficient methods for deoxygenation.[1] In recent decades, catalytic aldehyde decarbonylation has attracted significant interest as an effective method for the deoxygenation of organic compounds.[2] Decarbonylation provides a hydrogen-free alternative to hydrogenolysis in upgrading the octane and energy density of potential biofuels.[3] The decarbonylation of biomass-derived aldehydes, such as furfural and 5-hydroxymethylfurfural (HMF), also offers atom and energy efficient routes to valuable platform chemicals, such as furan and furfuryl alcohol (FFA) (Scheme 1).[4] However, HMF is a challenging substrate for decarbonylation due to its propensity to form oligomers and poorly defined polymers (humins) at elevated reaction temperatures in polar solvents.

There are only a handful of examples of catalytic decarbonylation using either homogeneous or heterogeneous catalysts. Homogeneous decarbonylation catalysts are primarily based on Rh,[5] Ru,[6] Ir,[7] and Pd[8] complexes. Although some operate under relatively mild conditions, most require high catalyst loading

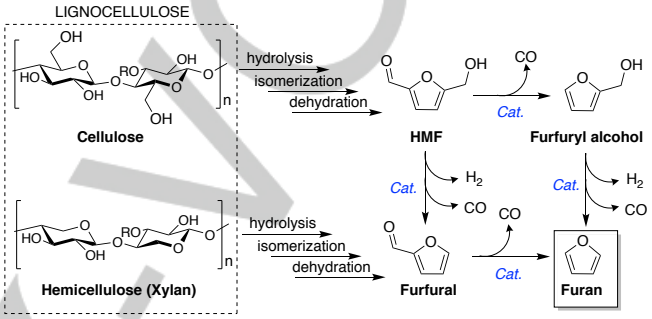


**Scheme 1.** Decarbonylation strategy for converting lignocellulose to platform chemicals HMF, furfural, furfuryl alcohol and furan.

(from 0.5 mol% for Ir[9] to 16 mol% for heptanal decarbonylation over Pd).[8a] In a recent example, Hu et al reported the tandem dehydration-decarbonylation of fructose using a Lewis acid for dehydration (aluminum chloride) and palladium acetate for decarbonylation, but required 11 mol% Pd to achieve full conversion with a turnover frequency (TOF) of only ~3 $h^{-1}$.[10] Heterogeneous catalysts reported for HMF and furfural decarbonylation are all Pd-derived (**Scheme 2**), but require significant improvements in efficiency (TOF range from 1–26 $h^{-1}$) and robustness.

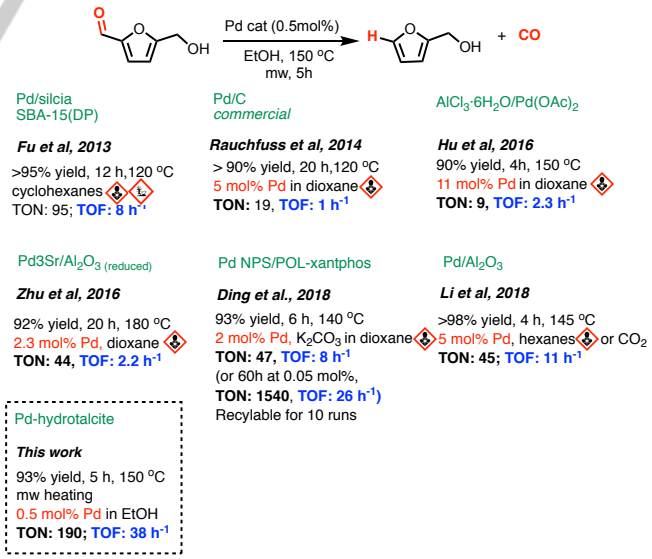


**Scheme 2**. Heterogeneously catalyzed HMF decarbonylation.

The earliest example, a commercial Pd/charcoal catalyst, was active for furfural decarbonylation at 170 °C; however, activity was strongly dependent on the type of charcoal and also sensitive to

[a] N. An, D. Ainembabazi, C. Reid, K. Samudrala, A. Voutchkova-Kostal;
Chemistry Department
The George Washington University
880 22nd St NW, Washington, D.C. 20052, USA
E-mail: avoutchkova@gwu.edu
[b] K. Wilson, A. F. Lee;
Applied Chemistry & Environmental Science
RMIT University, Melbourne, Australia
Email: adam.lee2@rmit.edu.au; karen.wilson2@rmit.edu.au

trace acid.[4, 11] Silica supported Pd catalysts (Pd/SBA-15 and Pd/fibrous silica)[12] were also reported for HMF decarbonylation employing 1 wt% and 5 mol% Pd respectively; however, further catalyst optimization was not achieved (**Scheme 2**). In contrast, Li et al showed that doping Pd/alumina with alkali earth metals tuned both Pd dispersion and charge density, and in turn decarbonylation activity.[13]

The above literature precedents suggest that potential improvements to catalytic activity may arise from the use of basic[4] and tunable supports[13] that afford high metal dispersion. Given our prior work on a class of palladium catalysts incorporating tunable hydrotalcite (HT) solid bases,[14] we sought to explore whether these may offer advantageous activity and selectivity for the decarbonylation of biomass-derived and synthetic aldehydes. HTs are a subset of layered double hydroxides (LDHs) composed of metal hydroxide sheets sandwiched by weakly bound anions and water.[15] Naturally occurring HT consists of $Mg^{2+}$ and $Al^{3+}$ hydroxides in the cationic layer and carbonate anions in the interlayers, but synthetic analogs can be prepared by isomorphically substituting $Mg^{2+}$ and $Al^{3+}$ ions in the metal hydroxide sheets for isovalent metal ions with compatible ionic radii. Such substitution is important in two ways: first, it allows modulation of the surface acid/base,[16] redox,[17] and catalytic properties[18] of HTs with minimal impact on morphology;[19] and second, it facilitates the stabilization of highly dispersed metal ions in the HT matrix. Thus, HT-supported catalysts could serve as a useful platform for stabilizing dispersed catalytic species on supports possessing tunable electronic properties. We recently developed a highly reproducible synthesis route to Pd functionalized hydrotalcites (Pd-HTs) using co-precipitation under continuous flow.[20] These Pd-HTs have characteristics distinct from similar HT supported species obtained via post-synthetic deposition.[21] Herein, we describe the high activity of Pd-HTs synthesized in flow for selective aldehyde decarbonylation under microwave and conventional conditions, using low catalyst loadings and short reaction times, wherein activity and selectivity can be readily optimized. Microwave heating is advantageous in chemical synthesis[22] and biomass processing[23] due to direct reactant heating as compared to slow conductive and convective heat transfer by conventional heating. This catalytic system does not require a promoter, soluble base, or the exclusion of air or water, and provides a notable reduction in the precious metal loading and environmental impact compared to the state-of-the-art (Scheme 2).

## Results and Discussion

### Characterization of Pd-HTs

Pd-HTs were synthesized using a meso-scale continuous flow method previously described[14, 24] (**Figure S1**), which yields materials with reproducible elemental composition, surface area, and acid-base properties. Four Pd-HT catalysts (***A***, ***B***, ***C*** and ***D***) were synthesized with nominal loadings of 5, 1, 0.5 and 0.1 mol% Pd by varying the metal precursor concentrations (**Table S1**). A fifth pure HT (***E***) was synthesized as a control by the same method. Elemental analysis by ICP-AES showed that the actual metal compositions were within 0.8 % of the nominal values (**Table S2**). Increasing the Pd loading from 0 to 4.7 mol% only induced a small (but systematic) decrease in the Mg:Al ratio from 3.0 to 2.84 (**Table S2**).

Powder X-ray diffraction (XRD) patterns of the five HTs all evidenced a single hydrotalcite phase, with no detectable crystalline Pd or PdO phases (**Figure 1**). The lack of crystalline Pd phases, even at 5 mol% loading, suggests that palladium is highly dispersed, either as low nuclearity species or particles with sub-2 nm dimensions. The (*003*), (*006*), (*009*) reflections of the HT are sensitive to the interlayer spacing, while the (*110*) and (*113*) reflections are related to the average metal-metal distance within the metal cation layers. Consistent *a* and *c* parameters (**Table S2** for crystallographic parameters) for all the HTs suggests that Pd functionalization had negligible impact on the underlying support structure; crystallite sizes determined by the Scherrer equation were also consistent across all samples (10.5 ± 0.2 STD). BET surface areas and pore volumes determined by nitrogen porosimetry increased systematically with decreasing Pd loading from 53 $m^2/g$ to 148 $m^2/g$, attributed to partial blockage of micropore entrances to the interlayer spaces for higher loadings. FT-IR spectra were also indicative of a hydrotalcite phase, showing the expected stretches associated with interlayer carbonate anions ($\nu_{C=O}$ 1350 - 1370 $cm^{-1}$) and water ($\nu_{H-O-H}$ bending at 1400~1700 $cm^{-1}$) (**Figure S2**). The only feature that changed with increasing Pd loading was the intensity of the $\nu_{Pd-O}$ at 500 $cm^{-1}$. We recently reported that increasing the Pd content of Pd-HTs results in decreased basicity and increased acidity, suggesting that Pd species may associate with surface hydroxyls and introduce Lewis acidic $Pd^{\delta+}$ species,[25] and decreased thermal stability, possibly associated with greater structural disorder.

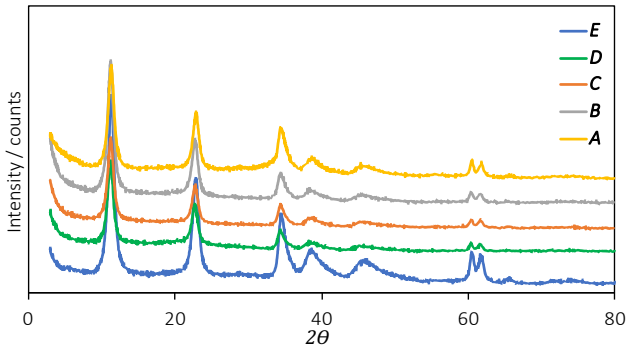


**Figure 1.** Powder XRD patterns of Pd-HT catalysts (***A*** – ***D***) and parent HT (***E***).

Pd surface speciation was investigated by X-ray photoelectron spectroscopy (XPS) (**Figure 2** and **Table S3**). No Pd signal was detectable for the 0.1% Pd-HT (***D***) sample due to the low metal content. Catalysts ***A***, ***B***, and ***C*** exhibited two common Pd chemical environments, one with a $3d_{5/2}$ binding energy of 335.4 eV characteristic of $Pd^0$ metal[26] and the second with a $3d_{5/2}$ binding energy of 336.8 eV characteristic of $Pd^{2+}$ in PdO.[27,14] A third chemical environment with a higher binding energy of 338.0 eV was also observed for ***C*** (0.5% Pd-HT) and is attributed to $Pd^{4+}$, although it is important to note that both initial[27] and final[28] state effects can also increase the binding energy of small metal clusters over conductive and insulating supports. The presence of multiple Pd species is unsurprising, given that HTs offer both framework and surface coordination environments. Highly oxidized (and dispersed) Pd species are not observed when functionalization is performed by post-synthetic immobilization of HTs or calcined HTs (mixed metal oxides), which favor nanoparticulate Pd (either as metal[21a, 21b] or oxide[21e]). The distribution of Pd surface species (**Figure 2b**) reveals a significant decrease in the proportion of $Pd^{4+}$, and concomitant rise in $Pd^{2+}$, with increasing loading. In contrast, the corresponding $Pd^0$ concentration shows only a small variance with Pd loading; this likely reflects the presence of an approximately constant proportion of (large) metallic nanoparticles, although this variation is also consistent with a growth mode reported by Matolin and Stara over alumina, in which highly dispersed Pd species initially present subsequently agglomerate into 3D clusters before re-dispersing as 2D islands.[29]

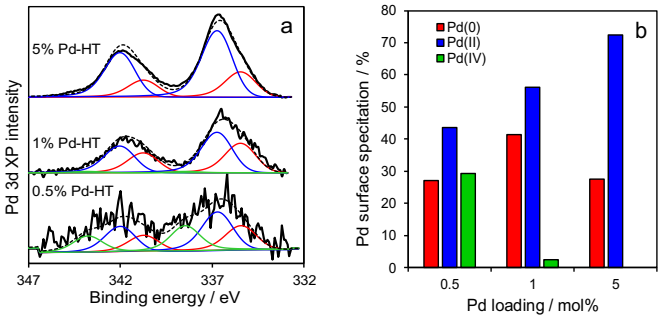


**Figure 2.** (a) Pd 3d XP spectra of Pd-HTs, and (b) corresponding fitted Pd speciation.

TEM images of ***A*** and ***B*** confirmed the presence of 1-2.5 nm nanoparticles (**Figure 3a-b** and **Figure S3**), consistent with XRD and XPS data. In contrast, no nanoparticles were observed for ***C*** or ***D*** (**Figure 3c-d**), although EDS mapping of ***D*** indicated a uniform Pd dispersion (**Figure 4e**). High resolution TEM images identified two types of NPs in ***A***: those with 0.227 nm lattice fringes corresponding to fcc Pd(111) facets; and those with 0.215 nm lattice fringes attributed to PdO(110) facets (**Figure S4**). Only metallic Pd nanoparticles were identified for ***B***. Considering the XPS and TEM measurements, and the ionic radii data of Pd in different oxidation states, we propose that the 0.5% Pd-HT (***C***) consists of atomically dispersed $Pd^{4+}$ species incorporated into the HT cationic layers, and low nuclearity $Pd^{2+}$ species dispersed over the surface of HT layers. The 5% Pd-HT (***A***) comprised small PdO clusters and metallic Pd nanoparticles. Direct measurement of the Pd dispersion (surface:total atom ratio) by CO chemisorption was not possible since CO titrates both Pd metal and the basic hydrotalcite supports. Consequently, catalytic activity is quantitated based on the total Pd content, consistent with literature precedents,[30] and hence reported TONs could underestimate the true catalyst performance.

## Furfural decarbonylation

***Solvent optimization.*** Furfural and HMF decarbonylation is primarily reported in 1,4-dioxane (**Scheme 2**),[31] a polar aprotic solvent often used in lignocellulose pretreatment. However, the short-term acute toxicity of 1,4-dioxane (symptoms include vertigo, drowsiness, anorexia, and ear/nose/lung irritation), and long-term effects resulting from chronic exposure (such as hepatotoxicity, neurotoxicity and carcinogenicity in animal models)[32] suggest dioxane is not suitable for the sustainable, large scale processing of biomass. The development of greener methods for lignocellulose pretreatment, such as the lignin-first ethanolsolv process,[33] pave the way for decarbonylation using a bio-derived and less hazardous solvent, such as ethanol. A solvent screen was therefore first conducted using catalyst ***A*** to direct solvent selection, with reactions performed using closed vials and microwave heating to mitigate boiling point limitations and enable comparison at the same temperature (150 °C); the potential advantages and limitations of microwave heating for biomass transformation were recently reviewed.[34]

Preliminary results using 0.5 mol% ***A*** (relative to furfural) showed that GVL and *p*-xylenes were poor solvents, with furan yields <15 %, whereas ethanol and 2-propanol deliver yields of

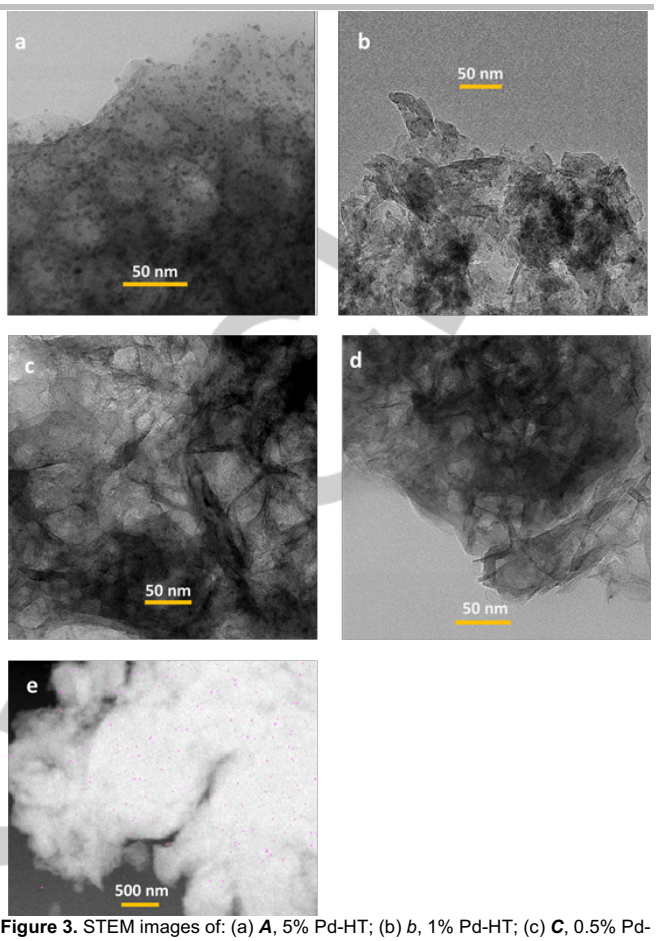


**Figure 3.** STEM images of: (a) ***A***, 5% Pd-HT; (b) *b*, 1% Pd-HT; (c) ***C***, 0.5% Pd-HT; (d) ***D***, 0.1% Pd-HT at 50 nm scale, and (e) EDS Pd mapping of ***D*** (Large image is shown in Figure S3).

82 % and 63 % respectively after 5 h at 150 °C (**Table S5**). Reaction in ethanol was also completely selective to furan; in contrast 2-propanol afforded ~12 % furfuryl alcohol arising from transfer hydrogenation. This may reflect the higher solubility of furfural in alcohols than *p*-xylenes, and/or solvent reduction of $Pd^{\delta+}$ to $Pd^{0}$. The latter is implicated in catalyst activation[35]: primary alcohols, such as ethanol and *n*-butanol, can reduce $Pd^{\delta+}$ via β-hydride elimination, unlike tertiary alcohols such as *t*-butanol. Indeed, furfural decarbonylation in *t*-butanol, which has similar polarity and microwave absorptivity to ethanol, afforded only a 15 % furan yield, supporting the notion of solvent-induced catalyst activation. Solventless decarbonylation at the same catalyst loading (0.5 mol%) was also evaluated, resulting in a furan yield of 45 % after 6 h and 72 % after 24 h. The low catalyst loading and high selectivity under neat conditions suggest scope for further optimization, for example by reactive distillation. For practical purposes ethanol was chosen as the optimal solvent for reaction at 150 °C; at 110 °C furan yields decreased to 55 %, while at 160 °C no significant improvement in yield was observed relative to 150 °C reaction. Microwave heating delivered superior conversion and furan yields to conventional heating in a closed vial, with the latter requiring 8 h to achieve 85 % furan (versus only 5 h under microwave irradiation) consistent with slower conduction and convection heat transfer.[34]

***Catalyst screening for furfural.*** The performance of catalysts ***A***-***D*** was subsequently explored for furfural decarbonylation under these optimized conditions (**Figure 4a**). The parent HT was inactive under our conditions. Control reactions without catalyst afforded no conversion to furan, with ~10 % yield of acetal product.

Furan was the major product in all cases, with furfuryl alcohol the major by-product (arising from catalytic transfer hydrogenation from ethanol, **Scheme 3**). Minute amounts of furoic acid were also observed, arising from hydration-dehydrogenation of the carbonyl due to residual water in the solvent. Product yields were uncorrelated with one another, evidencing independent reaction pathways. Furan production decreased slightly with decreasing Pd loading, with catalyst ***A*** (5%Pd-HT) offering 82 % and complete selectivity to furan. Commercial Pd/C performed poorly (18 % furan and 6 % furfuryl alcohol), while only 25 % furan was obtained using a homogeneous $Pd(OAc)_2$ catalyst. The furan yield was directly proportional to the surface concentration of Pd(II) species (**Figure 4b**), while that of furfuryl alcohol was only weakly correlated with surface Pd(0) (**Figure S5**). This relationship is consistent with the conclusions of the DFT study from Vlachos et al, which describe the furfural reduction to furfuryl alcohol as being kinetically favored over Pd(111), but decarbonylation to furan as thermodynamically more favorable.[36] Mechanistically, there is a small kinetic barrier to hydrogenation of the carbonyl oxygen in furfural to form furfuryl alcohol over Pd(111), which in turn may undergo facile hydrogen-assisted OH removal to 2-methylfuran (not observed in the present study). In contrast, furan production from furfural (and furfuryl alcohol) is predicted to occur through initial dehydrogenation to an acyl intermediate over palladium surfaces,[36-37] prior to C-C scission (decarbonylation), consistent with experimental temperature-programmed desorption studies for furfural[37] and aliphatic aldehydes.[38]

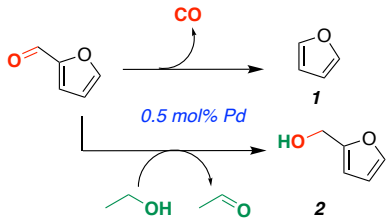


**Scheme 3.** Furfural decarbonylation to furan (***1***) or transfer hydrogenation to furfuryl alcohol (***2***).

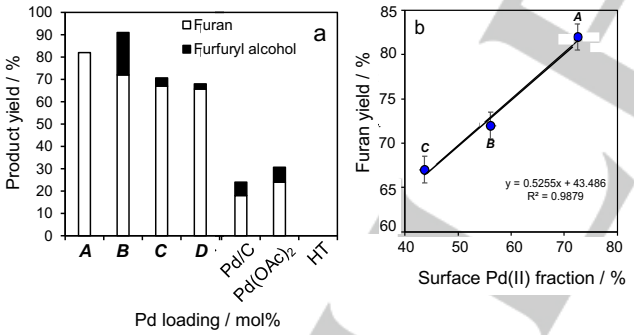


**Figure 4.** (a) Furan and furfuryl alcohol yields for furfural decarbonylation over Pd-HT catalysts and controls, and (b) relationship between surface Pd(II) species (from XPS) and furan production. Reaction conditions: 1 mmol furfural, 3 mL ethanol, 0.5 mol% Pd catalyst, 5 h, 150 °C, and microwave heating (200 W), under air.

***Evolved gas.*** When reactions were performed in air, the evolved gas was identified as $CO_2$, rather than CO (**Figure S6**). In contrast, under inert atmosphere conditions, CO was evolved in an approximately constant amount. This suggests that CO produced by direct aldehyde decarbonylation undergoes catalytic oxidation in air to $CO_2$. However, to exclude the possibility that the aldehyde was first oxidized to a carboxylic acid, which undergoes subsequent decarboxylation, benzoic acid was reacted with catalyst ***A*** under standard reaction conditions. No reaction was observed, confirming that the catalyst is not active for decarboxylation. Thus, the reactively-formed $CO_2$ must arise from catalytic CO oxidation. Supported Pd catalysts are widely reported for CO oxidation, for example Ladas et al observed high CO oxidation activity over dispersed Pd nanoparticles on $Al_2O_3$.[39]

## HMF decarbonylation

5-hydroxymethylfurfural (HMF) may undergo a broader range of metal-, acid- or base-catalyzed transformations, including decarbonylation (**Scheme 4**), dehydrogenation, transfer hydrogenation, hydrogenolysis and hydration-dehydrogenation. HMF may also undergo undesirable polymerization to humins, although these were not observed in the present work using ethanol as a solvent in the absence of additional water, i.e. anhydrous conditions were not required. However, humin formation was observed when ethanol was intentionally spiked with water (**Figure S7** shows TEM images of catalyst ***A*** and reactor residue post-reaction).

Effective conversion of HMF to value added products requires control over reaction selectivity. In addition to decarbonylation of the acyl group, the primary alcohol group may dehydrogenate to form an aldehyde, which can undergo further decarbonylation. The product distribution for HMF in the presence of catalysts ***A-D*** in ethanol at 150 °C was therefore quantified and compared with that for alternative Pd catalysts (**Figure 5**). As for furfural, the parent HT was inactive, and both homogeneous palladium acetate and the heterogeneous Pd/C catalysts offered poor (<30 %) yields of decarbonylation products; significant humin was also produced for the acetate. Note that the source (supplier) of Pd/C strongly influenced the reaction outcome due to variability in physicochemical properties. In contrast, all Pd-HTs gave furfuryl alcohol yields between 75-95 %. Catalyst ***A*** was highly selective for furfuryl alcohol, affording only trace amounts of furfural and 5-(hydroxymethyl)-2-furoic acid in a few reactions, whereas catalysts ***B*** – ***D*** produced 5-10 % by-products (furfural, furan and bis(hydroxymethyl) furan). As observed for furfural in **Figure 4**, the decarbonylation product yield was directly proportional to the surface concentration of Pd(II) species (**Figure 5b**); this suggest a common Pd(II) active site for furfural and HMF decarbonylation. ***A*** affords 92 % furfuryl alcohol and <3 % furfural, with no humin formation in 5 h, while ***C*** and ***D*** afford 75 and 74 % yield of furfuryl alcohol respectively in 5 h. Catalyst ***A*** was also tested using conventional heating of a sealed tube, but required 20 h to achieve 88 % yield (albeit the reaction temperature inside the tube was found to be 140 °C, rather than 150 °C). Control reactions without catalyst afforded no conversion to HMF.

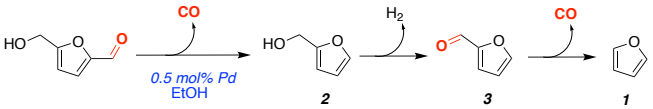


**Scheme 4.** HMF decarbonylation and subsequent dehydrogenation-decarbonylation to furfural (***3***) and furan.

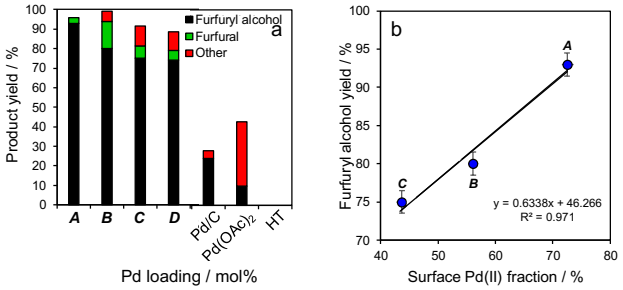


**Figure 5.** (a) Product yields for HMF decarbonylation over Pd-HT catalysts and controls ('other' includes furan (***1***) and humins), and (b) relationship between surface Pd(II) species (from XPS) and furfuryl alcohol production. Reaction conditions: 1 mmol HMF, 3 mL ethanol, 0.5 mol% Pd catalyst, 5 h, 150 °C, and microwave heating (200 W), under air.

## Benzaldehyde decarbonylation

Akin to furfural, benzaldehyde can also undergo decarbonylation and/or transfer hydrogenation in the presence of a hydrogen donor solvent such as ethanol (**Scheme 5**). However, decarbonylation was the dominant pathway over all Pd-HT catalysts, which achieved comparable benzene yields of 48-59 %. Catalyst ***A*** was again the most selective for decarbonylation (**Figure 6a**), and the decarbonylation product (benzene) yield was found to be proportional to surface Pd(II) (**Figure 6b**). Although $Pd(OAc)_2$ (and the parent HT) again exhibited poor activity towards the aldehyde substrate, in this instance Pd/C outperformed Pd-HTs for benzaldehyde decarbonylation.

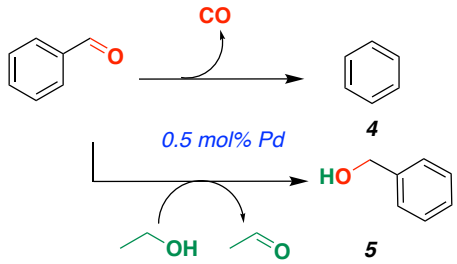


**Scheme 5.** Benzaldehyde decarbonylation to benzene (***4***) and competing transfer hydrogenation to benzyl alcohol (***5***) in ethanol.

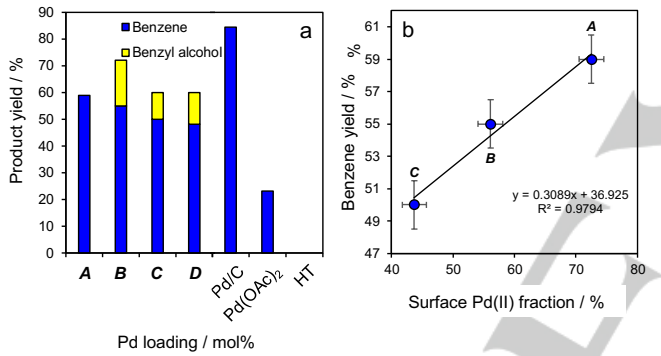


**Figure 6.** (a) Benzene and benzyl alcohol yields for benzaldehyde decarbonylation over Pd-HT catalysts and controls; (b) relationship between surface Pd(II) species (from XPS) and benzene production. Conditions: 1 mmol benzaldehyde, 3 mL ethanol, 0.5 mol% Pd catalyst, 5 h, 150 °C, microwave heating (200 W), under air.

The substrate scope of catalyst ***A*** was subsequently investigated for substituted benzaldehydes, with 50-99 % yields of the desired decarbonylation products obtained in all cases except for aryl halides (**Figure 7**), which readily undergo competing oxidative addition. Benzaldehydes with electron-withdrawing groups afforded the highest yields (e.g. *p*-nitrobenzaldehyde, 99 %), whereas those with electron-donating groups were least reactive (e.g. *p*-anisaldehyde, 37 %). Cinnamaldehyde was converted to styrene quantitatively in only 2 h (**Figure 7**).

The increased reactivity of benzaldehydes possessing electron-withdrawing groups was explored computationally. Madsen et al recently showed that the selectivity of homogeneous Rh species[40] for the decarbonylation of para-substituted benzaldehydes correlates with Hammett parameters.[40b] Halogenated benzaldehydes were an exception, and were better fitted by splitting the $\sigma$ values into resonance and inductive contributions. To understand whether the Pd-catalyzed process follows a similar trend, and develop a more general computational model to predict relative catalytic activity, we explored the relationship between Mulliken charge on the carbonyl carbon,

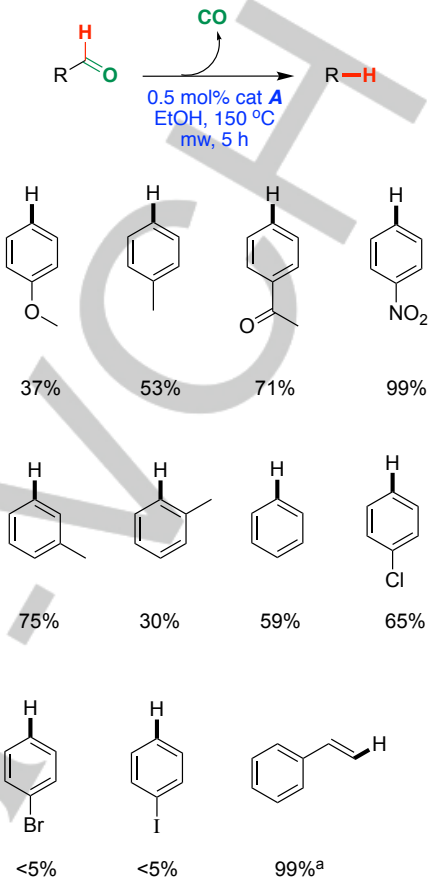


**Figure 7.** Substrate scope for benzaldehydes using catalyst ***A***. Reaction conditions: 1 mmol aldehyde, 3 mL ethanol, 0.5 mol% catalyst ***A***, 5h, 150 °C, microwave heating (200 W), under air. [a]Reaction time 2 h reaction.

calculated using density functional theory (B3LYP/6-31G(d)), and average reaction rate. The latter was calculated as the average rate of formation of decarbonylation product over the course of the reaction (**Table S6**). The carbonyl carbon charge is related to the C-H bond dissociation energy, which in turn influences the rate of C-H oxidative addition of the acyl group, the likely rate-determining step in decarbonylation. The Mulliken charge on the carbonyl carbon was directly proportional to the reaction rate for substituted benzaldehydes and cinnamaldehyde (**Figure 8**); note that iodo- and bromobenzaldehydes were excluded since they afforded no decarbonylation product due to competing reactivity at the C-X bond. This relationship indicates that negative charge accumulates in the rate-determining step of the reaction, consistent with the formation of a new metal-carbon bond with reactively-formed CO during C-C scission of a surface acyl intermediate.[36-37] The carbonyl charge may also be a surrogate for the C-C(O)H bond strength of the aldehyde which relates to the ability to eliminate CO after C-H oxidative addition. In the Rh-catalyzed reaction studied by Madsen et al, calculated energy paths suggest that CO and reductive elimination are much slower than oxidative addition, and thus more likely rate-limiting.

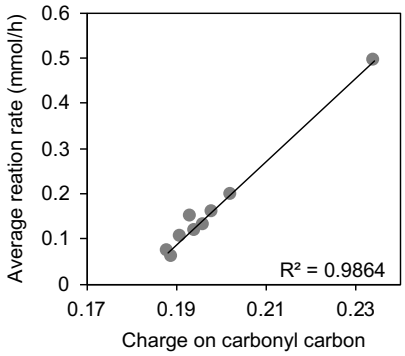


**Figure 8.** Correlation between Mulliken charge on the carbonyl carbon of substituted benzaldehydes and cinnamaldehyde and the decarbonylation rate over catalyst *A* (see **Table S6** for further details).

## Aliphatic aldehyde decarbonylation

Aliphatic aldehydes heptanal and phenacetaldehyde were also examined under neat conditions, however the major products afforded were not the result of direct decarbonylation. Since these substrates possess α-methylene groups, they can undergo aldol condensations in the presence of solid bases such as hydrotalcites. In both cases, subsequent decarbonylation of the aldol condensation product affords the E-alkene in 45% and 74 % yield respectively (**Scheme 6**). The fact that the direct decarbonylation products of the aldehydes are minor (5 % and 10 % respectively of heptane and toluene respectively) suggests that aldol condensation is faster than decarbonylation for these catalysts. Given the exciting nature of this new transformation, its substrate scope and applications will be explored further in a future report.[41]

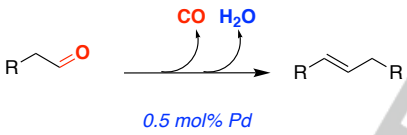


R = butyl, benzyl

**Scheme 6.** Decarbonylation of aliphatic aldehydes.

## Catalyst stability

***Poisoning tests.*** To examine whether decarbonylation was heterogeneously catalyzed or driven by soluble (leached) Pd species, we performed quantitative poisoning tests using 1,10-phenanthroline as a scavenger of soluble Pd.[42] The relative impact of this scavenger on cinnamaldehyde decarbonylation was compared for catalyst ***A*** versus commercial 5% Pd/C. Addition of stoichiometric 1,10-phenanthroline (relative to Pd) significantly reduced the activity of Pd/C, which was completely deactivated in the presence of 5 equivalents of the scavenger; in contrast, catalyst ***A*** only lost 20 % of its activity in the presence of such an excess (**Figure 9**). Hence aldehyde decarbonylation appears to operate largely through a homogeneous catalytic reaction involving leached Pd species for Pd/C, but a predominantly heterogeneous catalytic mechanism for Pd-HT (***A***).

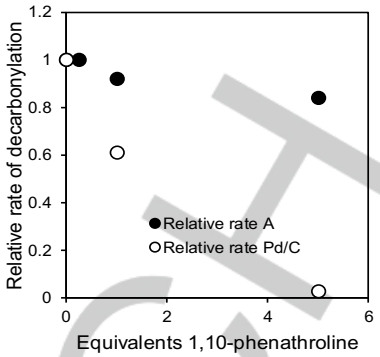


**Figure 9.** Poisoning test using 1,10-phenanthroline on decarbonylation of cinnamaldehyde, catalyzed by *A* and 5% Pd/C. (Conditions: 1 mmol cinnamaldehyde, 3 mL ethanol, 1 h at 150 °C, microwave heating).

***Characterization post-reaction.*** The Pd content of catalysts ***A*** – ***D*** and Pd/C post-reaction was determined by ICP-AES (**Table S7**) after reaction with HMF. That for Pd/C fell to 32 % of the original value post-reaction, however the loss for Pd-HTs was significantly smaller, and decreased with decreasing Pd loading in the case of ***B*** and ***C***. These results are consistent with the results of poisoning tests (see "Poisoning tests"), which showed more significant Pd leaching for Pd/C than catalyst ***A***. HRTEM shows that the mean size of Pd/PdO species in the used catalyst ***A*** increased from 1.84 nm to 2.76 nm after use (Figure S8), with a corresponding broader distribution of particle sizes. In addition, HRTEM identified two Pd phases: reduced Pd(111), and PdO(101), in contrast to the phases identified for the fresh catalyst (Pd(111) and PdO(110).

## Catalytic testing under continuous flow conditions

Since microwave reactions are not always readily scalable, we opted to translate the preceding chemistry to a continuous flow reactor. The numerous advantages of flow versus batch reactions have been extensively reviewed.[43] The activity and stability of catalyst ***A*** were explored under continuous flow for HMF decarbonylation (**Scheme 7**). Flow parameters were selected based on extrapolation from batch conditions, using a flow rate of 0.1 mL/min, 160 °C reaction temperature, and 10 bar $N_2$ (see ESI for full experimental details and reactor configuration **Figure S9**).

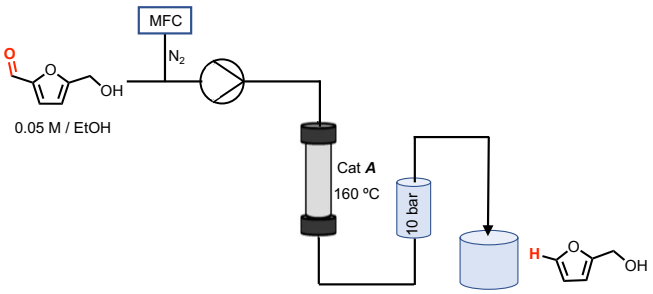


**Scheme 7.** Continuous flow decarbonylation of HMF using catalyst ***A*** (5%Pd-HT).

Under these conditions near-quantitative HMF conversion was observed, which remained fairly constant for 10 h on stream (**Figure 10**). The selectivity for furfuryl alcohol started low but increased to a steady state value of >90 % over several hours, suggesting that the catalyst has an induction period for decarbonylation. Given that batch experiments showed that decarbonylation activity is most strongly related to surface Pd(II) abundance for all substrates, we postulate that catalyst activation consists of solvent-assisted reduction of $Pd^{\delta+}$ to $Pd^0$, most likely forming smaller and more reactive Pd(111) species than those formed during catalyst synthesis. This is consistent with recent

reports implicating small size in the high activity of Pd clusters for similar processes.[44]

By-products observed during this induction period include bis(hydroxymethyl) furan and 5-(hydroxymethyl)-2-furoic acid, respectively arising from transfer hydrogenation and hydration-dehydrogenation of the aldehyde due to residual water in the ethanol. At steady state, furfuryl alcohol productivity reached 645.8 μmol.g$^{-1}$.h$^{-1}$. The catalyst was then cooled to room temperature overnight, and re-tested at 130 °C for a subsequent 7 h. Stable and high conversion (83-94 %) and furfuryl alcohol selectivity (66-78 %) were immediately attained, consistent with the catalyst pre-activation; the same by-products were observed as at the higher reaction temperature. ICP-AES revealed that only 10 % of the initial Pd was lost over 17 h reaction on-stream (**Table S7**); this small amount is consistent with heterogeneously catalyzed decarbonylation, as observed in batch (**Figure 9**).

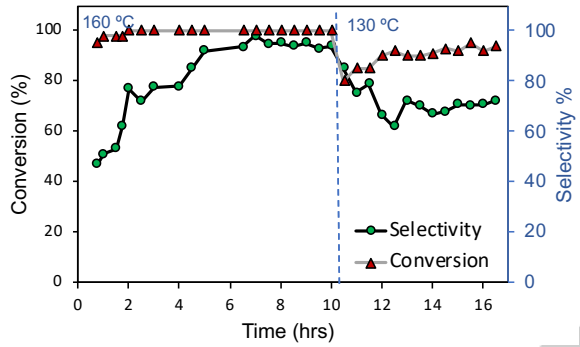


**Figure 10.** Continuous flow HMF decarbonylation using catalyst ***A*** (5% Pd-HT). Conditions: 0.05 M HMF in ethanol, 160 °C, 0.1 mL/min flow rate, 10 bar $N_2$, residence time ~2 min.

The significance of Pd leaching from catalyst ***A*** in batch reactions merits some additional discussion. **Figures 4-6** evidence only a small change in total product yield with Pd loading for furfural, HMF and benzaldehyde decarbonylation, despite a 50-fold reduction in the amount of Pd between catalysts ***A*** and ***D***. Furthermore, no quantifiable leaching was apparent by ICP-AES for the latter 0.1% Pd-HT (catalyst D). These findings strongly indicate that leached Pd makes negligible contribution to the observed catalysis, i.e. decarbonylation is overwhelmingly heterogeneously catalysed, consistent with: (i) the low activity and selectivity of soluble Pd species in all our $Pd(OAc)_2$ control reactions; (ii) 1,10-phenanthroline 'poisoning' tests (**Figure 9**) which demonstrate that catalyst ***A*** retained 80 % of its initial activity despite scavenging of leached Pd species; and the excellent stability of catalyst ***A*** in continuous flow conditions (**Figure 10**) under which leached Pd is removed from the reactor (which would result in rapid deactivation if the catalytic reaction was homogeneous). It is worth recalling that the observation of leaching from a solid is an essential, but not sufficient, condition to prove a homogeneous contribution to catalysis. The body of evidence overwhelming suggests our Pd-HT catalysts operate by a heterogeneous mechanism; Pd weakly bound to the HT support in catalyst ***A*** may leach during reaction, but is catalytically inactive.

## Conclusions

A family of Pd-HT catalysts was prepared by flow synthesis. Structural and textural properties of the parent HT (Mg:Al = 3:1) were retained in all cases, however Pd particle size and oxidation state was a strong function of metal loading: ≤0.5 mol% Pd favours highly dispersed $Pd^{2+}$ and $Pd^{4+}$, likely associated with low nuclearity clusters and atomically dispersed species within the cationic layers respectively; higher loadings favor PdO nanoparticles. Pd-HT catalysts were efficient for the decarbonylation of furfural, HMF, and aromatic aldehydes (other than aryl halides) under relatively mild microwave conditions. Activity and selectivity to the desired decarbonylation products slightly increased with Pd loading for substrates, with Pd-HT catalysts significantly outperforming commercial Pd/C and $Pd(OAc)_2$ controls in almost all cases. Decarbonylation performance was a strong function of solvent selection. Alcohols with β-hydrogens, such as ethanol and 2-propanol, proved most effective, possibly through catalyst activation by *in-situ* reduction of $Pd^{2+}$; decarbonylation product yields were proportional to the initial $Pd^{2+}$ surface concentration in the as-prepared Pd-HT. Minor by-products arose predominantly from either transfer hydrogenation (furfural and benzaldehydes) or dehydrogenation-decarbonylation (HMF). In contrast to commercial Pd/C, which underwent significant Pd leaching during reaction, 5%Pd-HT exhibited good stability during HMF decarbonylation in both batch and continuous flow operation.

**Keywords:** aldehydes, decarbonylation, heterogeneous catalysis, hydrotalcite, palladium

## References

[1] G. J. S. Dawes, E. L. Scott, J. Nôtre, J. P. M. Sanders, J. H. Bitter, *Green Chemistry* **2015**, *17*, 3231-3250.

[2] a)J. A. Lopez-Ruiz, R. J. Davis, *Green Chemistry* **2014**, *16*, 683-694; b)D. Necas, M. Kotora, *Curr Org Chem* **2007**, *11*, 1566-1591.

[3] a)A. Schirmer, M. A. Rude, X. Z. Li, E. Popova, S. B. del Cardayre, *Science* **2010**, *329*, 559-562; b)N. Li, H. Norgaard, D. M. Warui, S. J. Booker, C. Krebs, J. M. Bollinger, *J. Am. Chem. Soc.* **2011**, *133*, 6158-6161.

[4] P. Lejemble, A. Gaset, P. Kalck, *Biomass* **1984**, *4*, 263-274.

[5] a)D. H. Doughty, L. H. Pignolet, *J. Am. Chem. Soc.* **1978**, *100*, 7083-7085; b)C. Chapuis, B. Winter, K. H. Schultelte, *Tetrahedron Lett.* **1992**, *33*, 6135-6138; c)F. Abuhasanayn, M. E. Goldman, A. S. Goldman, *J. Am. Chem. Soc.* **1992**, *114*, 2520-2524; d)C. M. Beck, S. E. Rathmill, Y. J. Park, J. Chen, R. H. Crabtree, L. M. Liable-Sands, A. L. Rheingold, *Organometallics* **1999**, *18*, 5311-5317; e)P. Fristrup, M. Kreis, A. Palmelund, P. O. Norrby, R. Madsen, *J. Am. Chem. Soc.* **2008**, *130*, 5206-5215.

[6] G. Domazetis, B. Tarpey, D. Dolphin, B. R. James, *J Chem Soc Chem Comm* **1980**, 939-940.

[7] a)F. M. A. Geilen, T. vom Stein, B. Engendahl, S. Winterle, M. A. Liauw, J. Klankermayer, W. Leitner, *Angew Chem Int Edit* **2011**, *50*, 6831-6834; b)T. Iwai, T. Fujihara, Y. Tsuji, *Chem. Commun.* **2008**, 6215-6217.

[8] a)A. Modak, A. Deb, T. Patra, S. Rana, S. Maity, D. Maiti, *Chemical Communications* **2012**, *48*, 4253-4255; b)Akanksha, D. Maiti, *Green Chemistry* **2012**, *14*,

2314-2320; c)B. F. M. Kuster, *Starch-Starke* **1990**, *42*, 314-321.

[9] F. M. A. Geilen, T. vom Stein, B. Engendahl, S. Winterle, M. A. Liauw, J. Klankermayer, W. Leitner, *Angewandte Chemie International Edition* **2011**, *50*, 6831-6834.

[10] J. H. Dai, X. Fu, L. F. Zhu, J. Q. Tang, X. W. Guo, C. W. Hu, *Chemcatchem* **2016**, *8*, 1379-1385.

[11] J. Mitra, X. Y. Zhou, T. Rauchfuss, *Green Chemistry* **2015**, *17*, 307-313.

[12] a)Y. B. Huang, Z. Yang, M. Y. Chen, J. J. Dai, Q. X. Guo, Y. Fu, *Chemsuschem* **2013**, *6*, 1348-1351; b)P. K. Kundu, M. Dhiman, A. Modak, A. Chowdhury, V. Polshettiwar, D. Maiti, *Chempluschem* **2016**, *81*, 1142-1146.

[13] Q. W. Meng, C. W. Qiu, G. Q. Ding, J. L. Cui, Y. L. Zhu, Y. W. Li, *Catal Sci Technol* **2016**, *6*, 4377-4388.

[14] D. Ainembabazi, N. An, J. C. Manayil, K. Wilson, A. F. Lee, A. M. Voutchkova-Kostal, *Acs Catal* **2019**, *9*, 1055-1065.

[15] a)D. G. Evans, R. C. T. Slade, in *Layered Double Hydroxides, Vol. 119* (Eds.: X. Duan, D. G. Evans), Springer-Verlag Berlin, Berlin, **2006**, pp. 1-87; b)L. P. F. Benício, R. A. Silva, J. A. Lopes, D. Eulálio, R. M. M. d. Santos, L. A. d. Aquino, L. Vergütz, R. F. Novais, L. M. d. Costa, F. G. Pinto, J. Tronto, *Revista Brasileira de Ciência do Solo* **2015**, *39*, 1-13.

[16] D. Meloni, M. F. Sini, M. G. Cutrufello, R. Monaci, E. Rombi, I. Ferino, *Journal of Thermal Analysis and Calorimetry* **2011**, *108*, 783-791.

[17] E. Scavetta, M. Berrettoni, M. Giorgetti, D. Tonelli, *Electrochim Acta* **2002**, *47*, 2451-2461.

[18] F. S. Bert, E. D. V. Dirk, A. J. Pierre, *Catalysis Reviews* **2001**, *43*, 443488.

[19] F. Cavani, F. Trifiro, A. Vaccari, *Catal Today* **1991**, *11*, 173-301.

[20] P. Yaseneva, N. An, M. Finn, N. Tidemann, N. Jose, A. Voutchkova, A. Lapkin, *Abstr Pap Am Chem S* **2018**, *256*.

[21] a)B. M. Choudary, S. Madhi, N. S. Chowdari, M. L. Kantam, B. Sreedhar, *J. Am. Chem. Soc.* **2002**, *124*, 14127-14136; b)M. I. Burrueco, M. Mora, C. Jimenez-Sanchidrian, J. R. Ruiz, *Appl Catal a-Gen* **2014**, *485*, 196-201; c)T. H. Bennur, A. Ramani, R. Bal, B. M. Chanda, S. Sivasanker, *Catalysis Communications* **2002**, *3*, 493-496; d)M. Mora, C. Jimenez-Sanchidrian, J. R. Ruiz, *J Mol Catal a-Chem* **2008**, *285*, 79-83; e)D. Naresh, V. P. Kumar, M. Harisekhar, N. Nagaraju, B. Putrakumar, K. V. R. Chary, *Appl Surf Sci* **2014**, *314*, 199-207; f)Z. Y. Wu, Q. Q. Zhu, C. Shen, T. W. Tan, *Acs Omega* **2016**, *1*, 498-506.

[22] M. A. Herrero, J. M. Kremsner, C. O. Kappe, *The Journal of Organic Chemistry* **2008**, *73*, 36-47.

[23] E. Ahmad, M. I. Alam, K. K. Pant, M. A. Haider, *Industrial & Engineering Chemistry Research* **2019**.

[24] P. Yaseneva, N. An, M. Finn, N. Tidemann, N. Jose, A. Voutchkova, A. Lapkin, *Continuous Synthesis of Doped Layered Double Hydroxides in a Meso-Scale Flow Reactor*, **2018**.

[25] G. Strukul, *Topics in Catalysis* **2002**, *19*, 33-42.

[26] J. F. Moulder, J. Chastain, R. C. King, *Handbook of x-ray photoelectron spectroscopy : a reference book of standard spectra for identification and interpretation of XPS data*, Physical Electronics, Eden Prairie, Minn., **1995**.

[27] S. Peters, S. Peredkov, M. Neeb, W. Eberhardt, M. Al-Hada, *Surface Science* **2013**, *608*, 129-134.

[28] a)A. Fritsch, P. Légaré, *Surface Science* **1985**, *162*, 742-746; b)G. K. Wertheim, S. B. DiCenzo, *Physical Review B* **1988**, *37*, 844-847.

[29] V. Matolin, I. Stara, *Surface Science* **1998**, *398*, 117-124.

[30] a)A. Corma, P. Concepcion, M. Boronat, M. J. Sabater, J. Navas, M. J. Yacaman, E. Larios, A. Posadas, M. A. Lopez-Quintela, D. Buceta, E. Mendoza, G. Guilera, A. Mayoral, *Nat Chem* **2013**, *5*, 775-781; b)J. K. Edwards, G. J. Hutchings, *Angew Chem Int Ed Engl* **2008**, *47*, 9192-9198; c)S. J. F. Nishtha Agarwal, Rebecca U. McVicker, Sultan M. Althahban, Nikolaos Dimitratos, Qian He, David J. Morgan, Robert L. Jenkins, David J. Willock, Stuart H. Taylor, Christopher J. Kielu, Graham J. Hutchings, *Science* **2017**, *358*, 4.

[31] a)J. Mitra, X. Zhou, T. Rauchfuss, *Green Chemistry* **2014**, *17*, 307-313; b)W. H. Li, C. Y. Li, Y. Li, H. T. Tang, H. S. Wang, Y. M. Pan, Y. J. Ding, *Chem. Commun.* **2018**; c)Y. B. Huang, Z. Yang, M. Y. Chen, J. J. Dai, Q. X. Guo, Y. Fu, *Chemsuschem* **2013**, *6*, 1348-1351; d)J. Dai, X. Fu, L. Zhu, J. Tang, X. Guo, C. Hu, *Chemcatchem* **2016**, *8*, 1379-1385.

[32] U. S. E.P.A., HSDB Database, **2018**, pp. https://toxnet.nlm.nih.gov/cgi-bin/sis/search/a?dbs+hsdb:@term+@DOCNO+81.

[33] D. S. Zijlstra, A. de Santi, B. Oldenburger, J. de Vries, K. Barta, P. J. Deuss, *Jove-J Vis Exp* **2019**.

[34] P. Priecel, J. A. Lopez-Sanchez, *Acs Sustain Chem Eng* **2019**, *7*, 3-21.

[35] P. R. Melvin, D. Balcells, N. Hazari, A. Nova, *Acs Catal* **2015**, *5*, 5596-5606.

[36] V. Vorotnikov, G. Mpourmpakis, D. G. Vlachos, *Acs Catal* **2012**, *2*, 2496-2504.

[37] S. H. Pang, J. W. Medlin, *Acs Catal* **2011**, *1*, 1272-1283.

[38] J. L. Davis, M. A. Barteau, *J. Am. Chem. Soc.* **1989**, *111*, 1782-1792.

[39] S. Ladas, H. Poppa, M. Boudart, *Surface Science* **1981**, *102*, 151-171.

[40] a)P. Fristrup, S. Le Quement, D. Tanner, P. O. Norrby, *Organometallics* **2004**, *23*, 6160-6165; b)M. Kreis, A. Palmelund, L. Bunch, R. Madsen, *Advanced Synthesis & Catalysis* **2006**, *348*, 2148-2154.

[41] D. Ainembabazi, C. Reid, A. Voutchkova, *Submitted*.

[42] E. Bayram, R. G. Finke, *Acs Catal* **2012**, *2*, 1967-1975.

[43] a)T. N. Glasnov, C. O. Kappe, *Chemistry – A European Journal* **2011**, *17*, 11956-11968; b)M. B. Plutschack, B. Pieber, K. Gilmore, P. H. Seeberger, *Chemical Reviews* **2017**, *117*, 11796-11893.

[44] a)T. Ishida, *Journal of catalysis* **2019**, *v. 374*, pp. 320-327-2019 v.2374; b)T. Ishida, K. Kume, K. Kinjo, T. Honma, K. Nakada, H. Ohashi, T. Yokoyama, A. Hamasaki, H. Murayama, Y. Izawa, M. Utsunomiya, M. Tokunaga, *Chemsuschem* **2016**, *9*, 3441-3447.

10.1002/cssc.201901934

WILEY-VCH



# FULL PAPER

Nan An[a], Diana Ainembabazi, Christopher Reid, Kavya Samudrala, Karen Wilson, Adam F. Lee*, Adelina Voutchkova-Kostal*

***Page No. – Page No.***

**Microwave-assisted Decarbonylation of Biomass-derived Aldehydes using Pd-doped Hydrotalcites**

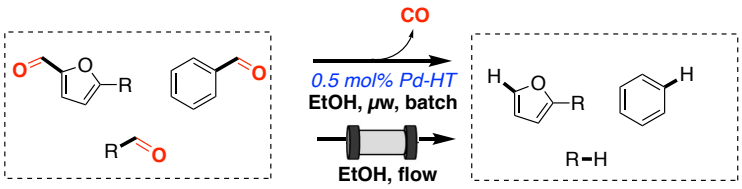






[a] N. An, D. Ainembabazi, C. Reid, K. Samudrala, A. Voutchl